

JPL Document D-73329

# ***TECHNOLOGY DEVELOPMENT FOR EXOPLANET MISSIONS***


*Technology Milestone White Paper  
Vortex Coronagraph Technology*

*Gene Serabyn, P.I.  
John Krist, Dimitri Mawet,  
Dwight Moody, and John Trauger*

***23 March 2012***

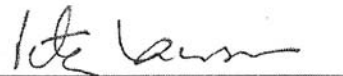
**Approvals:**

Released by

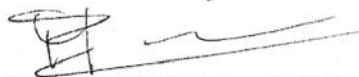
  
Gene Serabyn  
Principal Investigator

5-10-2012  
Date

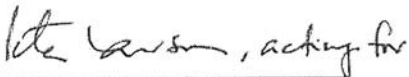
Approved by

  
Peter Lawson  
Exoplanet Exploration Program Chief Technologist, JPL

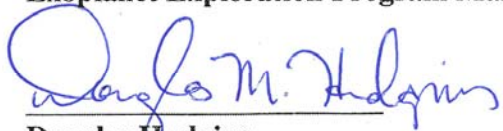
5/11/12  
Date

  
Marie Levine  
Exoplanet Exploration Program Technology Manager, JPL


5/11/12  
Date

  
Michael Devirian  
Exoplanet Exploration Program Manager, JPL

5/14/12  
Date

  
Douglas Hudgins  
Exoplanet Exploration Program Scientist, NASA HQ

5/15/12  
Date

  
Lia LaPiana  
Exoplanet Exploration Program Executive, NASA HQ

5/15/12  
Date

# Table of Contents

<b>1. Objective .....</b>	<b>3</b>
<b>2. Introduction.....</b>	<b>3</b>
2.1. Relevance for a Future Exoplanet Mission .....	4
2.2. The Vortex Coronagraph.....	5
2.3. Vortex Masks .....	6
2.4. HCIT configuration .....	9
2.5. Differences Between Flight and Laboratory Demonstrations.....	10
<b>3. Computation of the Metric .....</b>	<b>11</b>
3.1. Definitions .....	11
3.2. Measurement of the Star Brightness .....	13
3.3. Measurement of the Coronagraph Contrast Field .....	13
3.4. Milestone Demonstration Procedure .....	15
<b>4. Success Criteria.....</b>	<b>16</b>
<b>5. Certification.....</b>	<b>17</b>
5.1. Milestone Certification Data Package.....	17
<b>6. References.....</b>	<b>18</b>

# TDEM Milestone White Paper: Vortex Coronagraph Technology

## 1. Objective

In support of NASA's Exoplanet Exploration Program and the ROSES Technology Development for Exoplanet Missions (TDEM), this whitepaper explains the purpose of the first TDEM Milestone for *Demonstrations of Deep Starlight Rejection with a Vortex Coronagraph*, specifies the methodology for computing the milestone metrics, and establishes the success criteria against which the milestone will be evaluated. This milestone is concerned with a demonstration of monochromatic high contrast. Subsequent milestones will be aimed at demonstrating performance for more broadband light (10 – 20% bandwidth) and at smaller angles (to  $\approx 2$  diffraction beam widths), so as to attain performance levels required by space missions.

## 2. Introduction

TDEM Technology Milestones are intended to document progress in the development of key technologies for a space-based mission that would detect and characterize exoplanets, such as TPF-C (Levine et al. 2006), ACCESS (Trauger et al. 2010), or a smaller (to be defined) Explorer-class mission, thereby gauging the mission concept's readiness to proceed from pre-Phase A to Phase A.

This milestone addresses monochromatic starlight suppression. The objective of this TDEM milestone is the validation of a vortex focal plane mask with monochromatic (or narrowband) light. This milestone thus focuses on the validation of one key TDEM technology – the vortex mask. Success is defined in terms of statistically significant performance demonstrations of this key technology, ideally with minimal sensitivity or dependence on extraneous environmental factors.

Completion of this milestone is to be documented in a report by the Principal Investigator and reviewed by the Exoplanet Exploration Program.

This milestone reads as follows:

### **Milestone 1 definition: Narrowband Starlight Suppression with Vortex Masks**

*Using vortex masks, demonstrate a calibrated coronagraph contrast of  $1 \times 10^{-9}$  at angular separations of  $3 \lambda/D$  to  $8 \lambda/D$ , at a wavelength,  $\lambda$ , in the range 400 – 900 nm, for at least one polarization state.*

The “angular separations” are defined in terms of the wavelength  $\lambda$  and the diameter  $D$  of the aperture stop on the deformable mirror (DM), which is the pupil-defining element of the laboratory coronagraph. For this milestone, vortex masks will be used in an approximately  $f/50$  to  $f/100$  beam, corresponding to the current HCIT configuration with a pupil stop at the deformable mirror (DM) of at least 16 mm diameter. The minimum pupil diameter allows for the potential use of off-the-shelf polarization components, some

of which may vignette the beam at a diameter of somewhat under an inch.

## 2.1. Relevance for a Future Exoplanet Mission

Development of the vortex technology is intended to advance the readiness of a mission concept for the coronagraphic imaging and spectroscopic observation of exoplanetary systems. The small inner working angle capability of the vortex coronagraph allows consideration of a range of mission sizes, from several meter diameter flagship missions to much smaller, Explorer-class, missions.

To detect exoplanets in the super-Earth to Jovian range, a coronagraph must provide raw image contrast of  $\approx 10^{-9}$  in a dark field near the parent star. It is expected that post-processing of coronagraph data will provide detection sensitivities to planets and debris disks an order of magnitude fainter (Trauger and Traub 2007). Therefore, this milestone requires a demonstration of a high contrast dark field at the  $10^{-9}$  level.

Exoplanet imaging missions form a high contrast “dark field” over a working angle spanning  $n_i\lambda/D$  to  $n_{DM}\lambda/2D$ , where  $n_i$  sets the inner working angle, as defined by the science requirements, and  $n_{DM}$  is the number of actuators across the deformable mirror. An inner working angle of  $4\lambda/D$  was set by the TPF-C science requirements in the TPF-C STDT report (Levine et al. 2006), but smaller values are theoretically possible with the vortex coronagraph. The outer working angle ( $n_{DM}\lambda/2D$ ) is defined by the highest spatial frequency controlled by the deformable mirror (DM) aperture used. In our case, this aperture may initially be set by the size of easily available polarization components, but it will be large enough to allow dark holes at least out to  $8\lambda/D$ . (Polarization components will allow for some discrimination between error budget terms, and single-polarization vortex coronagraphs may in any case be required for reaching very high contrast.)

Extensive optical modeling and tolerancing has shown that it is increasingly difficult to control the contrast in the dark field as one moves closer to the image of the target star. This milestone begins to address the most challenging region of the image plane, at small angular separations. In fact, the first milestone will reach an inner working angle substantially smaller than that originally called for by TPF-C. On the other hand, the HCIT DM has 1024 actuators controlling the surface of a 32×32 mm mirror facesheet. Because of the sizes of polarization optics that may be incorporated, for this initial milestone we specify a beam at least 16 mm in diameter. This is of sufficiently large size that the physics of the wavefront control problem can be demonstrated with high expectation of applying the same approach to a larger dark field at a later date.

The contrast specification relates to the average contrast level in the dark field of interest around the source or parent star. This criterion was used in earlier HCIT milestones. It should be applicable to any coronagraph that propagates its image from sky to the coronagraph focal plane without optical distortions. Analysis of contrast in the dark field (if close to the target value) must necessarily account for the statistical nature of the static and “quasi-static” speckle patterns. The milestone measurements themselves will result in a distribution of speckle intensities, from which we will estimate the average contrast and statistical confidence levels. Statistical measures of both the average intensity and its variance in the coronagraph dark field will be provided in support of the milestone validation package, as specified in Section 5 below. If however, the result is well below the milestone target, the statistical analysis can be minimal.

## 2.2. The Vortex Coronagraph

Among the four major coronagraph types, the optical vortex coronagraph brings the advantages of a small inner working angle, high transmission, a clear off-axis field of view, and compatibility with the layout of the Lyot coronagraph (Guyon et al. 2006; Serabyn et al. 2010; Mawet et al. 2011).

The operation of an ideal optical vortex coronagraph is as follows (Mawet et al. 2005; Swarzlander 2009, Serabyn & Mawet 2012). A clear telescope input pupil can be described by a field distribution,  $P_i(r)$ , of

$$P_i(r) = \begin{cases} 1 & \text{for } r < A \\ 0 & \text{for } r > A, \end{cases} \quad (1)$$

where  $r$  is the radial coordinate, and  $A$  is the radius of the input aperture. Focusing the light leads, via a Fourier transform, to the usual focal-plane field distribution,

$$E_f(\theta) \propto \frac{J_1(kA\theta)}{kA\theta}, \quad (2)$$

where  $J_1$  is the Bessel function of order 1,  $k$  is the wavenumber, and  $\theta$  is the angular radial offset from the center of the stellar PSF.

Centering a transmissive vortex phase mask on this focal plane point spread function multiplies the ideal focal plane field distribution by a phase factor corresponding to an azimuthal phase ramp, i.e.,  $e^{in\alpha}$ , where  $\alpha$  is the azimuthal angle, and  $n$  is the ‘‘topological charge’’ of the vortex (i.e., the number of  $2\pi$ 's of phase the mask provides for one circuit about the center), yielding

$$E_f(\theta, \alpha) \propto e^{in\alpha} \frac{J_1(kA\theta)}{kA\theta}. \quad (3)$$

After passage through the focal plane vortex phase mask, the light is recollimated, and an image of the pupil is formed. This pupil arises by the usual Fourier transform relationship between focal and pupil planes, and because of the extra phase factor, and the properties of Bessel functions, specifically

$$J_n(x) = \int_{-\pi}^{\pi} e^{-i(n\phi - x\sin(\phi))} d\phi, \quad (4)$$

where  $J_n$  refers to Bessel functions of order  $n$ , for a second order vortex the final pupil plane distribution is proportional to (Mawet et al. 2005; Swarzlander 2009; Serabyn & Mawet 2012)

$$\int_0^{\infty} J_2(kr\theta)J_1(kA\theta)d\theta \quad (5)$$

instead of the usual

$$\int_0^{\infty} J_0(kr\theta)J_1(kA\theta)d\theta. \quad (6)$$

This seemingly slight change in the integrand has the effect of changing the resultant pupil distribution dramatically: instead of the original uniformly illuminated pupil (i.e., with all of the light inside the entrance pupil, and zero light outside the entrance pupil), a distribution with all of the light outside of the original pupil results, i.e., the reimaged region of the interior of the original pupil has uniformly zero intensity. In the post-vortex pupil, the electric field falls off as  $r^{-2}$  (Fig. 1, top right panel). In the ideal case, the starlight is then completely blocked by a simple opaque stop in the downstream pupil plane that is matched to the pupil radius. For higher order vortices, similarly clear pupil interiors ensue, but with different radial profiles beyond the original pupil radius. Of course with wavefront aberrations present, residual light will appear inside the pupil.

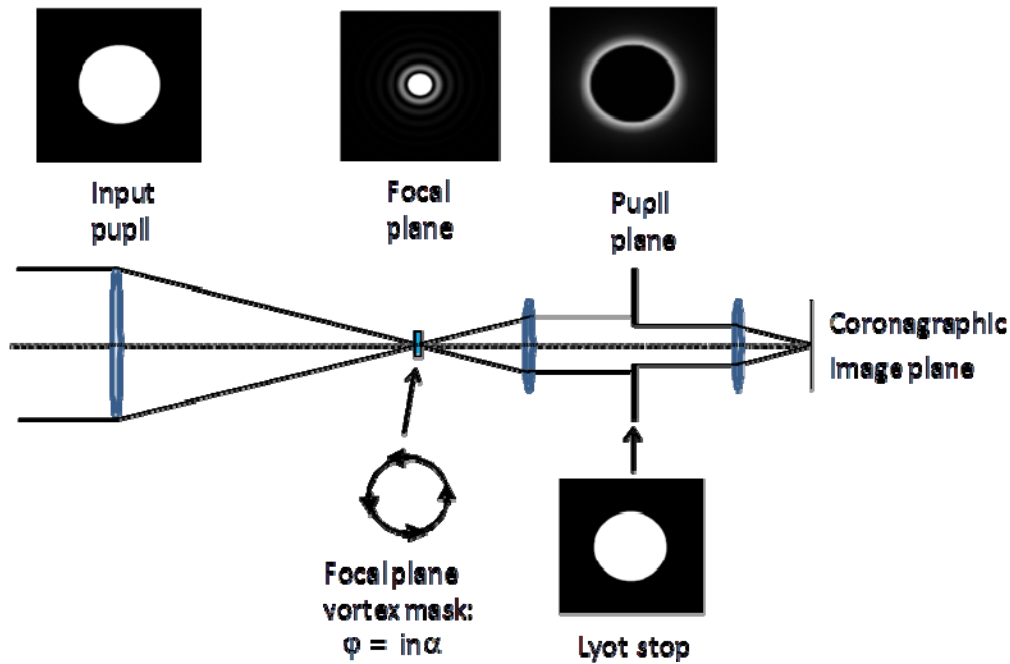


**Figure 1.** Layout of the optical vortex coronagraph: an optical vortex phase mask in the focal plane yields a downstream pupil image in which all of the on-axis starlight appears outside of the original pupil's image, where it is blocked by an aperture (Lyot) stop.

### 2.3. Vortex Masks

This TDEM award supports the testing of vortex masks in the HCIT and the corresponding modeling, but the vortex masks themselves will be developed, delivered and tested under a number of parallel work efforts, including a NASA Astrophysics Research and Analysis (APRA) grant to the PI, and an internal JPL grant to purchase a Mueller matrix polarimeter for device characterization. As our baseline plan, we will focus on the development and testing of vector vortex phase masks manufactured out of liquid crystal polymers (LCP). The properties of the fabricated masks will be characterized in detail (Figure 2) with, e.g., a polarizing microscope and a Mueller matrix polarimeter. Furthermore, to minimize valuable HCIT time, initial coronagraphic tests,

whenever possible, will be carried out on our Infrared Coronagraphic Testbed (IRCT), which actually operates into the visible regime as well.

Beyond the baseline plan of liquid crystal polymer masks, we will also have access to photonic crystal vortex masks produced by our Japanese colleagues (Mawet et al. 2011a), and it should be possible to fit in brief tests of these masks in the HCIT during schedule gaps. (Likewise, we will be investigating alternative approaches to manufacturing both scalar (longitudinal phase) and vector (geometric phase) vortex masks, under the APRA award, but that is not relevant here, unless one of the other alternatives has huge success). Thus, as stated in the TDEM proposal, none of these other mask types are part of our baseline plan, and they are viewed purely as a potential bonus. However, note that a comparison between two different types of vortex mask in the HCIT is likely to provide a very useful diagnostic comparison in practice, in some cases likely to aid in the discrimination between different leakage origins. Thus, we plan to include limited tests comparing different types of masks. A detailed discussion of the different types of vortex mask and of their relative advantages and disadvantages is provided in Mawet et al. (2011a).

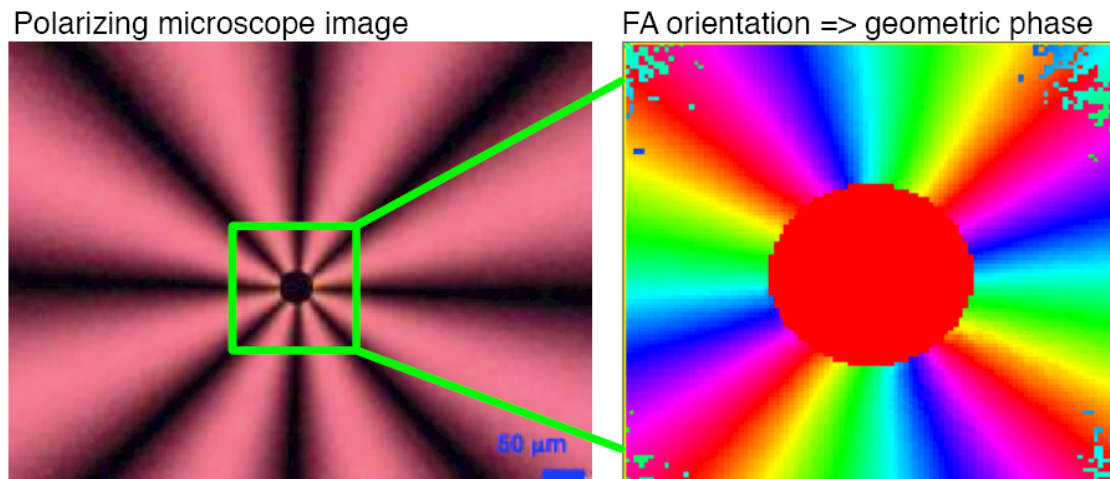


**Figure 2.** *Left: A fourth-order liquid crystal polymer vortex phase mask between crossed polarizers. Right: zoom on the central part using a polarimetric microscope, as measured at the Univ. of Arizona, showing the fast axis orientation rotating about the center. Here, this rotation yields a geometric phase change equals to  $4\theta$ , where  $\theta$  is the focal plane azimuthal coordinate, subsequently spanning 4 waves or  $8\pi$ . (Mawet et al. 2011b).*

Our current baseline LCP mask design, as developed in concert with JDSU, is shown in Figure 3 (Mawet et al. 2009). One such mask was already used for a quick initial test in the HCIT during an earlier fortuitous gap in the schedule (Mawet et al 2011a,b; Serabyn et al. 2012), and achieved single-polarization, monochromatic contrast of  $3.4 \times 10^{-9}$  over a region defined by cut-off hemisphere between  $2.5$  and  $12 \lambda/D$ , and with a contrast of  $\sim 10^{-8}$  in the innermost part of this region. This mask was not in the HCIT long enough to determine the origin of these limiting contrast values, so one of our primary goals here is to investigate the possible origins of the residual light leakage seen when operating this mask in the HCIT.



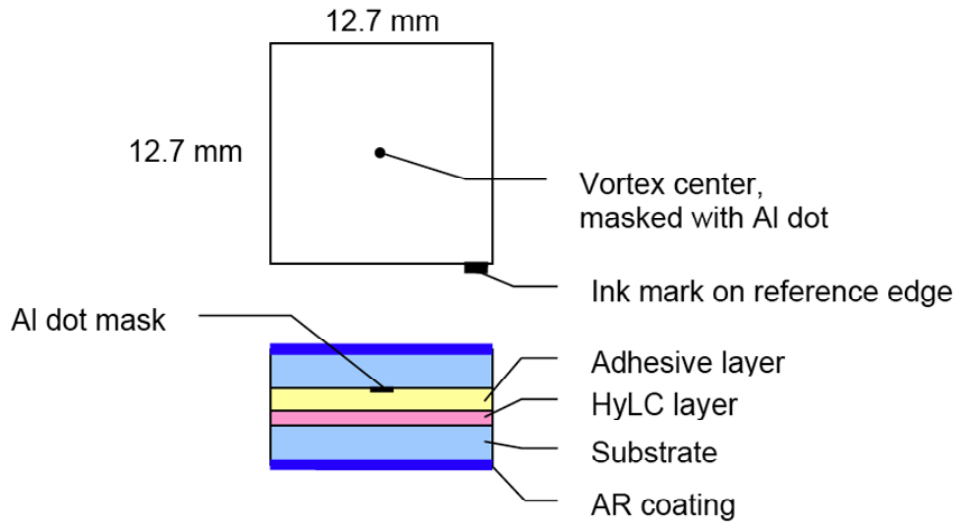


**Figure 3.** *Cross-section of the sandwich design of our current liquid crystal vortex masks. The hybrid liquid crystal polymer (HyLC) layer is deposited on one substrate and a small opaque dot mask is placed upon another substrate, and the two are then glued together, with the dot centered over the vortex.*

Limitations to the coronagraphic performance of vector vortex phase masks can arise in several ways, all of which lead to increased stellar leakage. The imperfections include both those in the phase masks themselves and those in the focal plane diffraction pattern that is coupled to the vortex phase mask. Mask imperfections can arise in imperfections in the geometrical orientations of the optical axes, a significant problem near the center of the vortex, in deviations from the necessary half-wave criterion, which is strictly met only at a number of design wavelengths, in extra (ghost) reflections from the optical interfaces within the vortex’s layered structure, and in irregularities in the materials themselves, which serve as scattering centers. On the other hand, even with a perfect vortex mask, extra starlight leakage will result if the diffraction point spread function deviates from a perfect Airy pattern positioned exactly on the center of the vortex. These issues are discussed in depth in Mawet et al. (2011a) and Serabyn & Mawet (2012). Understanding these issues will require modeling at both the device and system level, and validating our device level models is seen as part of this TDEM, as is the system-level coronagraph model for the vortex in the HCIT optical system, the latter based on the earlier modeling TDEM of Krist et al. (2010), which will allow us to probe system level error sensitivities. To test these error budget terms in practice, we will employ an array of standard optical tools for separating error budget terms, including polarizers, quarter wave plates, shutters, baffles, and varying beam apertures and wavelengths, among others.

Working with vendors, in some cases potentially through small business innovative research (SBIR) grants, our liquid crystal polymer mask designs will be upgraded to reduce issues associated with the factors listed above: the central “disorientation regions”, in which the vortex pattern is lost, ghost reflections from interfaces, and material quality and cleanliness issues. Finally, our future milestones involve an increase in the operating bandwidth (not important for Milestone 1).

## 2.4. HCIT configuration

The current optical layout of the HCIT Lyot table is shown in Figure 4, taken from Mawet et al. (2011b). The optical system resides in a vacuum chamber that can be evacuated to  $\sim 10$  milliTorr levels. Minor modifications to this configuration will likely be required to accommodate the various vortex TDEM demonstrations scheduled to take place on this table, as partially illustrated in Figure 4.

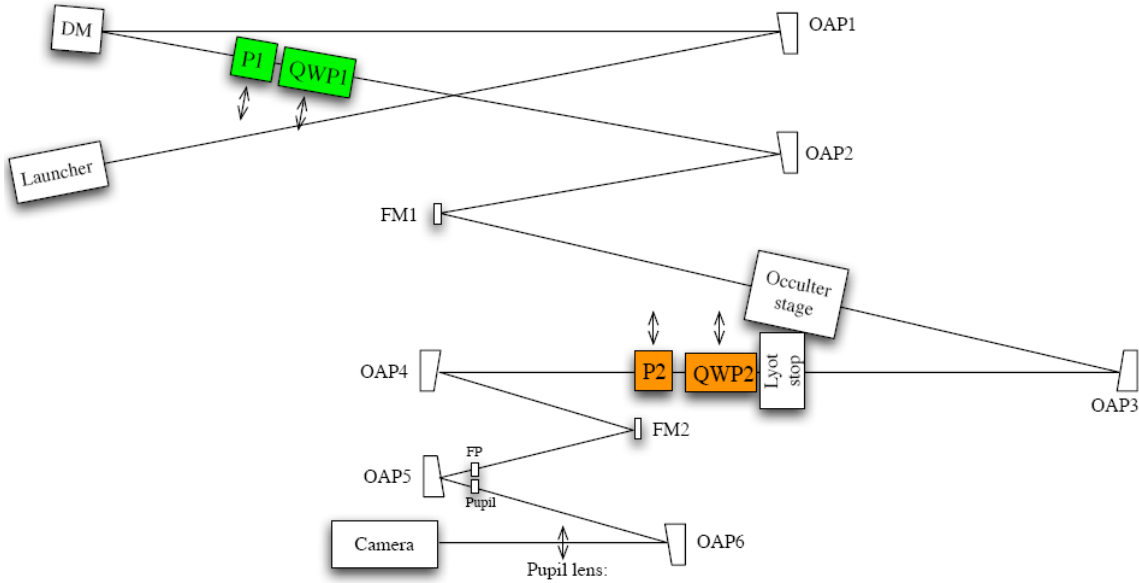


**Figure 4.** Optical layout of the HCIT coronagraph table with several (not all-inclusive) potential optical modifications for the vortex work shown in color. The optical elements, in the optical path starting from the source, are as follows. The light source illuminates OAP1, the first of six off-axis paraboloidal (OAP) mirrors, where the beam is collimated. The beam passes to the deformable mirror (DM), where an aperture stop defines the pupil of the system. The DM is from Xinetics, with 1024 actuators driving a mirror facesheet measuring  $32 \times 32$  mm. The collimated light is then focused by OAP2 and folded by the flat mirror FM1, passing to the focal plane where the vortex mask will be located. The beam is then collimated by OAP3 on its way to the Lyot stop, which is located in a pupil plane conjugate to the deformable mirror. The collimated beam is then brought to a focus by OAP4 to create the high-contrast coronagraph image, as indicated. A camera, formed by a pair of small OAPs, then magnifies and projects the coronagraph image onto the CCD focal plane. Rotatable and removable (by translation) polarizers (P) and quarter wave plates (QWP) will be inserted, as shown in color, to select and analyse the radiation, and a final analyser (not shown) may be added as well.

The first milestone demonstration will rely on a wavefront sensing and correction process that has been used in previous high-contrast demonstrations, including our earlier brief vortex experiment in the HCIT. A variant of the “electric field conjugation method” (EFC), as described in Give’on *et al.* (2007), is used and iterated repeatedly as necessary,

as follows. For a given wavelength, and starting with a nominally flat surface figure setting on the DM, we will: (a) take a set of contrast field images with the initial DM setting; (b) take images for each of four “probe” DM settings (consisting of small deterministic surface figure deviations from the initial DM setting), (c) use these data to compute the complex electric field in the target dark field region; and then (d) calculate and apply a new DM setting that will reduce the energy over the dark field, thus establishing a new “initial DM setting” in preparation for the next iteration, which is a loop back to step (a). A typical integration time for an individual image is about 10 sec, and one complete wavefront sensing and control cycle, including overhead for CCD readouts, data handling and computations, typically takes 10-15 minutes.

## 2.5. Differences Between Flight and Laboratory Demonstrations

There are several important differences between the lab demonstration and flight implementation. Each is addressed briefly below.

**Starlight:** In a space coronagraph, the spectrum of light illuminating the coronagraph would closely resemble black body radiation. For this first milestone, the source would be a monochromatic laser (or in the best case, narrowband [i.e., ~ 1% - 2%] light). The laser provides a photon flux that is comparable to or somewhat brighter than the target stars to be observed. The goal of this milestone is to demonstrate the contrast that can be achieved, independent of the source intensity. A bright source is a convenience that does not compromise the integrity of the demonstration, as it affects only the integration times.

Moreover, unlike the light collected by a telescope from a target star, the light intensity is not uniform across the pupil. Typically this non-uniformity is a center-to-edge “droop” of a few percent corresponding to the diffraction pattern from a small pinhole. This small level of non-uniformity is expected to have negligible effect on the final contrast if it is accounted for in the wavefront control algorithm, and is expected to result in a finite but below-requirement loss of contrast if it were ignored in the control algorithm.

**Spacecraft dynamics:** A control system is required in flight to stabilize the light path against motions of the spacecraft. The dominant effects of spacecraft dynamics are jitter of the star image on the coronagraph focal plane mask and beam walk in the optics upstream of the focal plane mask. For a specific example, the ACCESS analysis showed that for fourth-order coronagraphs (including Lyot, vortex, and pupil mapping coronagraphs) with an inner working angle of  $3\lambda_0/D$ , that pointing errors needed to be less than  $\pm 0.03 \lambda_0/D$  rms to limit the corresponding contrast degradation to less than  $2 \times 10^{-10}$ . The concept models have shown that the required pointing stability can be achieved in space with current high Technology Readiness Level (TRL) systems. Scaled to the HCIT, this would correspond to an ability to center the vortex mask on the “star” within  $2 \mu\text{m}$ , or about 0.4 pixel when projected to the CCD focal plane.

The milestone demonstration requires the passive stability of the testbed, including the centration of the star on the vortex as one example, which is untraceable to spacecraft dynamics. In practice, the HCIT often exhibits alignment drifts that are larger than expected in the space environment. As such we must rely on favorable periods of thermal and mechanical stability of the HCIT. Records of temperature variations in the HCIT for the time period spanning the duration of the experiments will be useful in this regard, and if available will be recorded during the milestone demonstrations described in

this whitepaper.

**Single deformable mirror:** The milestone demonstrations will be carried out with a single DM, which allows the control of phase and amplitude in the complex wavefront over one half of the coronagraph field described. In flight, it is expected that a pair of DMs will be used, in series, to generate a full (two-sided) dark field, with the added advantages of a deeper contrast field and better broadband control.

On the other hand, with the exception of the second DM, and the actual size of the DM, the layout of the vortex coronagraph in the HCIT is essentially the same as is being proposed for space (ACCESS; Trauger et al. 2010). The layout will also allow us to probe the need to separate polarization states to reach high contrast.

## 3. Computation of the Metric

### 3.1. Definitions

The contrast metric requires a measurement of the intensity of speckles appearing within the dark field, relative to the intensity of the incident star. The contrast metric will be assessed in terms of statistical confidence to capture the impact of experimental noise and uncertainties. In the following paragraphs we define the terms involved in this process, spell out the measurement steps, and specify the data products.

**3.1.1.** “Raw” Image and “Calibrated” Image. Standard techniques for the acquisition of CCD images are used. We define a “raw” image to be the pixel-by-pixel image obtained by reading the charge from each pixel of the CCD, amplifying and sending it to an analog-to-digital converter. We define a “calibrated” image to be a raw image that has had background bias subtracted and the detector responsivity normalized by dividing by a flat-field image. Saturated images are avoided in order to avoid the confusion of CCD blooming and other potential CCD nonlinearities. All raw images are permanently archived and available for later analysis.

**3.1.2.** We define “scratch” to be a DM setting in which actuators are set to a predetermined surface figure that is approximately flat (typically, about 20 volts on each actuator).

**3.1.3.** We define the “star” to be a small pinhole illuminated with laser or narrowband light relayed via optical fiber from a source outside the HCIT vacuum wall (e.g., a laser or a filtered super-continuum white light source). The “small” pinhole is to be unresolved by the optical system; e.g., a 5- $\mu\text{m}$  diameter pinhole would be “small” and unresolved by the 80- $\mu\text{m}$  FWHM Airy disk in an f/100 beam at 800 nm wavelength. This “star” is the only source of light in the optical path of the HCIT. It is a stand-in for the star image that would have been formed by a telescope system.

**3.1.4.** We define the “algorithm” to be the computer code that takes as input the measured speckle field image, and produces as output a voltage value to be applied to each element of the DM, with the goal of reducing the intensity of speckles.

**3.1.5.** The “contrast field” is a dimensionless map representing, for each pixel of the detector, the ratio of its value to the value of the peak of the central PSF that would be measured in the same testbed conditions (light source, exposure time, Lyot stop, etc.) if

the coronagraph focal plane mask were removed. The calibration of the contrast field is further detailed in Section 3.3.

**3.1.6.** The “contrast value” is a dimensionless quantity that is the average value of the contrast field over the dark field adopted for the experiment.

**3.1.7.** “Statistical Confidence”. The interpretation of measured numerical contrast values shall take into consideration, in an appropriate way, the statistics of measurement, including detector read noise, photon counting noise, and dark noise.

The milestone objective is to demonstrate with high confidence that the true contrast value in the dark field, as estimated from our measurements, is equal to or better than the required threshold contrast value  $C_0$ . The estimated true contrast value shall be obtained from the average of the set of four or more contrast values measured in a continuous sequence (over an expected period of approximately one hour).

For this milestone the required threshold is a mean contrast value of  $C_0 = 1.0 \times 10^{-9}$  with a confidence coefficient of 0.90 or better. Estimation of this statistical confidence level requires an estimation of variances. Given that our speckle fields contain a mix of static and quasi-static speckles (the residual speckle field remaining after the completion of a wavefront sensing and control cycle, together with the effects of alignment drift following the control cycle), as well as other sources of measurement noise including photon detection statistics and CCD read noise, an analytical development of speckle statistics is impractical. Our approach is to compute the confidence coefficients on the assumption of Gaussian statistics, but also to make the full set of measurement available to enable computation of the confidence levels for other statistics.

At any time in the demonstration, the true contrast is subject to laboratory conditions, including the quality of the optical components, their alignment, any drift in their alignment over time, and the effectiveness of each wavefront sensing and control cycle. With each iteration, our nulling procedure attempts to improve the contrast value, thus compensating for any drift or changes in alignment that may have occurred since the previous iteration, and further variations may be expected due to experimental noise and any limitations in the algorithm. The data set built up from a sequence of such iterations will provide a distribution of contrast values, which will be regarded as Gaussian about a mean contrast for the data set. We therefore consider the mean contrast value as representative of the true contrast value for a data set, and the distribution of contrast determinations among the iterations within the data set as a combination of both random wavefront control errors and random measurement errors.

The mean contrast values and confidence limits are computed in the following manner. The average of one or more images taken at the completion of each iteration is used to compute the contrast value  $c_i$ . The mean contrast for a set of images taken in a given sequence is:

$$\hat{c} = \sum_{i=1}^n \frac{c_i}{n}$$

where  $n$  is the number of images in each set. The standard deviation  $\sigma_{\text{each}}$  in the contrast values  $c_i$  obtained for individual images within the set, which now includes both the measurement noise and the (assumed random) contrast variations due to changes in the DM settings for each speckle nulling iteration, is:

$$\sigma_{each} = \sqrt{\frac{\sum_{i=1}^n (c_i - \hat{c})^2}{n-1}}$$

Our estimate  $\hat{c}$  is subject to uncertainty in the contrast measurements  $\sigma_{mean} = \sigma_{each} / \sqrt{n}$  and the independently-determined overall errors in photometry  $\sigma_{phot}$ . With the approximation that the contrast values have a Gaussian distribution about the mean contrast, the statistical confidence that the mean contrast is less than  $C_0 = 1 \times 10^{-9}$  is given by:

$$conf = \frac{1}{\sqrt{2\pi}} \int_{-\infty}^t e^{-z^2/2} dz$$

where  $t = (C_0 - \hat{c}) / \sigma$  and  $\sigma = \sqrt{\sigma_{mean}^2 + \sigma_{phot}^2}$ . The values  $\hat{c}$  and  $\sigma$  are the milestone metrics. The 90% confidence value is the value  $C_0$  such that  $conf(C_0) = 0.9$  according to the above equations.

## 3.2. Measurement of the Star Brightness

The brightness of the star is measured with the following steps.

**3.2.1.** The vortex mask is laterally offset by approximately  $10 \lambda/D$  or so, so as to transmit maximum stellar flux. Separately, the mask will be slowly stepped off axis and the radial throughput function measured.

**3.2.2.** To create the photometric reference, a representative sample of short-exposure (e.g. a few milliseconds) images of the star is taken, with all coronagraph elements other than focal-plane vortex mask in place.

**3.2.3.** The images are averaged to produce a single star image. The “short-exposure peak value” of the star’s intensity is estimated. Since the star image is well-sampled in the CCD focal plane (the Airy disk is sampled by  $\sim 20$  pixels within a radius equal to the full width half maximum), the star intensity can be estimated using either the value of the maximum-brightness pixel or an interpolated value representative of the apparent peak.

**3.2.4.** The “peak count rate” (counts/sec) is measured for exposure times of microseconds to tens of seconds.

## 3.3. Measurement of the Coronagraph Contrast Field

Each “coronagraph contrast field” is obtained as follows:

**3.3.1.** The vortex mask is centered on the star image.

**3.3.2.** An image (typical exposure times are  $\sim$  tens of seconds) is taken of the coronagraph field (the suppressed star and surrounding speckle field). The dimensions of the target areas, as shown schematically in Figure 5, are defined as follows: A dark (D-shaped) field extending from 3 to  $8 \lambda/D$ , representing a useful inner search space, is

bounded by a straight line that passes  $3 \lambda / D$  from the star at its closest point, and by a circle of radius  $8 \lambda / D$  centered on the star.

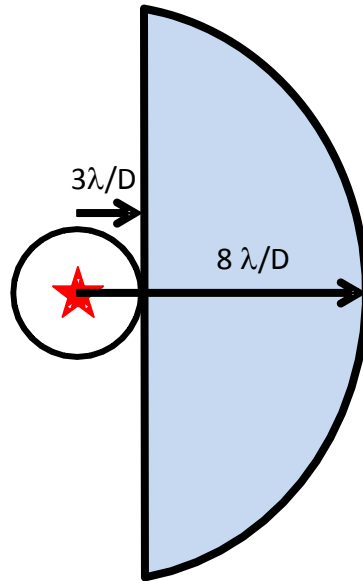


**Figure 5.** Target high-contrast dark field. As described in the text, inner and outer regions are defined for the one-sided dark field. The location of the suppressed central star is indicated in red. The target dark hole for this initial demonstration would be from  $3$  to  $8 \lambda / D$ , as defined in this figure.

**3.3.3.** The image is normalized to the “star brightness” as defined in 3.2. For this purpose, the fixed relationship between peak star brightness and the integrated light in the speckle field outside the central DM-controlled area will be established, as indicated in Figure 6 (taken from TPF-C Milestone Report #1, Trauger et al. 2006), providing the basis for estimation of star brightness associated with each coronagraph image.

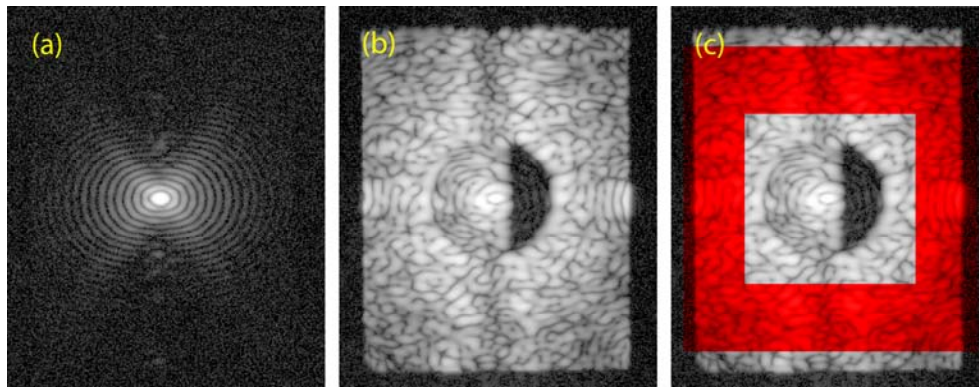


**Figure 6.** Reference fields for contrast photometry. Shown here are (a) the “star” reference image; (b) the high-contrast coronagraph field; and (c) superimposed in red

*is the reference speckle field in the “uncontrolled” area beyond the Nyquist limit for the deformable mirror. Images are displayed with a logarithmic contrast stretch.*

**3.3.4.** The contrast field image is averaged over the target high-contrast areas, to produce the contrast value. To be explicit, the contrast value is the sum of all contrast values, computed pixel-by-pixel in the dark field area, divided by the total number of pixels in the dark field area, without any weighting being applied. The rms contrast in a given area can also be calculated from the contrast field image.

### **3.4. Milestone Demonstration Procedure**

The procedure for the milestone demonstration is as follows:

**3.4.1.** The DM is set to scratch. An initial coronagraph contrast field image is obtained as described in Sec. 3.3.

**3.4.2.** Wavefront sensing and control is performed to find settings of the DM actuators that give the required high-contrast in the target dark field. This iterative procedure may take from one to several hours, starting from scratch, if no prior information is available. However it can take more or less time depending on the stability of the HCIT optical system.

**3.4.3.** A number of contrast field images are taken, following steps 3.3.1 – 3.3.2. The result at this point is a set of contrast field images. It is required that a sufficient number of images are taken to provide statistical confidence that the milestone contrast levels have been achieved, as described in Section 3.1.7 above.

**3.4.4.** Laboratory data are archived for future reference, including raw and calibrated images of the reference star and contrast field images.



## 4. Success Criteria

The following are the required elements of the milestone demonstration. Each element includes a brief rationale.

**4.1.** Illumination is monochromatic (or a few percent bandwidth) light in single or dual polarization at a wavelength in the range of  $400 \text{ nm} < \lambda < 900 \text{ nm}$ .

*Rationale: This milestone is an initial demonstration of the feasibility of the approach at a wavelength in the science band of TPF-C or ACCESS.*

**4.2.** A mean contrast metric of  $1 \times 10^{-9}$  or smaller shall be achieved in a 3 to 8  $\lambda/D$  dark zone, as defined in Sec. 3.3.2.

*Rationale: This provides evidence that the high contrast field is sufficiently dark ( $10^{-9}$  expected exozodi level) to be useful for searching planets, and to carry out initial tests at small angles.*

**4.3.** Criterion 4.2, averaged over the data set, shall be met with a confidence of 90% or better, as defined in Sec. 3.1.5. Sufficient data must be taken to justify this statistical confidence.

*Rationale: Assuming the contrast values have a Gaussian distribution about the mean contrast, this demonstrates a statistical confidence of 90% that the mean contrast goal has been reached.*

**4.4.** Elements 4.1 – 4.3 must be satisfied on three separate occasions with a reset of the wavefront control system software (DM set to scratch) between each demonstration.

*Rationale: This provides evidence of the repeatability of the contrast demonstration.*

*The wavefront control system software reset between data sets ensures that the three data sets can be considered as independent and do not represent an unusually good configuration that cannot be reproduced. For each demonstration the DM will begin from a "scratch" setting. There is no time requirement for the demonstrations, other than the time required to meet the statistics stipulated in the success criteria. There is no required interval between demonstrations; subsequent demonstrations can begin as soon as prior demonstrations have ended. There is also no requirement to turn off power, open the vacuum tank, or delete data relevant for the calibration of the DM influence function.*

## 5. Certification

The PI will assemble a milestone certification data package for review by the ExEPTAC and the ExEP program. In the event of a consensus determination that the success criteria have been met, the project will submit the findings of the review board, together with the certification data package, to NASA HQ for official certification of milestone compliance. In the event of a disagreement between the ExEP project and the ExEPTAC, NASA HQ will determine whether to accept the data package and certify compliance or request additional work.

### 5.1. Milestone Certification Data Package

The milestone certification data package will contain the following explanations, charts, and data products.

- 5.1.1. A narrative report, including a discussion of how each element of the milestone was met, and a narrative summary of the overall milestone achievement.
- 5.1.2. A description of the optical elements, including the vortex masks, and their significant characteristics.
- 5.1.3. A tabulation of the significant operating parameters of the apparatus.
- 5.1.4. A calibrated image of the reference star, and the photometry method used.
- 5.1.5. A calibrated image of the (distant) off-axis transmission of the vortex mask.
- 5.1.6. A contrast field image representative of the data set, with appropriate numerical contrast values indicated, with coordinate scales indicated in units of Airy distance ( $\lambda/D$ ).
- 5.1.7. For each image reported as part of the milestone demonstration, the average contrast recorded within the area spanning 3-4  $\lambda/D$ .
- 5.1.8. A description of the data reduction algorithms, in sufficient detail to guide an independent analysis of the delivered data.
- 5.1.9. Contrast metric values and supporting statistics for the overall data used to satisfy the milestone requirements, including a pixel-by-pixel histogram of contrast values across the dark field.

## 6. References

- Give'on, A., B. Kern, S. Shaklan, D. Moody, and L. Pueyo, "Broadband wavefront correction algorithm for high-contrast imaging systems," *Proc. SPIE* **6691**, 66910A, 2007.
- Guyon, O., Pluzhnik, E.A., Kuchner, M.J., Collins, B., and Ridgway, S.T. "Theoretical Limits On Extrasolar Terrestrial Planet Detection with Coronagraphs, *Ap.J. Suppl.* **167**, 81, 2006.
- Krist, J. et al., milestone report, 2012, in prep.
- Levine, M., Shaklan, S. & Kasting, J., "Terrestrial Planet Finder Coronagraph: Science and Technology Definition Team Report", JPL Publ. D-34923, 2006.
- Mawet, D., Riaud, P., Absil, O. and Surdej, J., "Annular Groove Phase Mask Coronagraph" *ApJ*, **633**, 1191, 2005.
- Mawet, D. Serabyn, E., Liewer, K., Hanot, Ch., McEldowney, S., Shemo, D. & O'Brien, N., "Optical Vectorial Vortex Coronagraphs using Liquid Crystal Polymers: Theory, Manufacturing and Laboratory Demonstration," *Optics Express*, **17**, 1902, 2009.
- Mawet, D. et al., "Taking the vector vortex coronagraph to the next level for ground- and space-based exoplanet imaging instruments: review of technology developments in the USA, Japan, and Europe," *Proc. SPIE* **8151**, 815108-1, 2011a.
- Mawet, D., et al. (2011b), "Recent Results of the Second Generation of Vector Vortex Coronagraphs on the High-contrast Imaging Testbed at JPL." *Proceedings of SPIE* **8151**, 81511D-8, 2011b.
- Serabyn E., D. Mawet & R. Burruss, "The potential of small space telescopes for exoplanet observations," E. Serabyn, *Proc. SPIE* **7731**, 77312O, 2010.
- Serabyn E., & Mawet, D. "Technology Development for Space Based Vortex Coronagraphy," *Proc. 2012 IEEE Aerospace Conf.*, Digital Object Identifier: [10.1109/AERO.2012.6187180](https://doi.org/10.1109/AERO.2012.6187180), 2012a.
- Serabyn, E. & Mawet, D., "Detecting Exoplanets with a Liquid-Crystal-Based Vortex Coronagraph," *Mol. Cryst. Liq. Cryst.*, **559**, 69, 2012b.
- Swartzlander, G., "The optical vortex coronagraph," *J. Opt. A.*, **11**, 1464, 2009.
- Trauger, J. et al., "TPF-C Milestone #1 Report," JPL Document D-35484, July 2006.
- Trauger, J. and W. Traub, "A laboratory demonstration of the capability to image an Earth-like extrasolar planet," *Nature* **446**, 771, 2007.
- Trauger, J., A. Give'on, B. Gordon, B. Kern, A. Kuhnert, D. Moody, A. Niessner, F. Shi, D. Wilson, and C. Burrows, "Laboratory demonstrations of high-contrast imaging for space coronagraphy," *Proc. SPIE* **6693**, 66930X, 2007.
- Trauger, J. et al., "ACCESS – A Concept Study for the Direct Imaging and Spectroscopy of Exoplanetary Systems," in Pathways towards Habitable Planets, *ASP Conf. Series* **430**, 375, 2010.